The Rigaku Journal
Vol. 18/ No. 1/ 2001

CONTRIBUTED PAPERS

APPLICATION OF THE IMAGING PLATE METHODOLOGY TO THE SOLUTION OF COMMENSURAT MODULATED STRUCTURES: IDENTIFICATION OF LONG-PERIOD MICA POLYTYPES BY X-RAY DIFFRACTION

MASSIMO NESPOLO

Japan Science and Technology Corporation, National Institute for Materials Science, 1-1 Namiki, Tsukuba-shi, lbaraki 305-0044 Japan

1. Introduction

The distinctive feature of modulated structures consists in the appearance of a series of satellite (commonly weaker) reflections surrounding the main (commonly stronger) reflections (basic structure reflections). In terms of the reciprocal cell of the basic structure, the satellite reflections may have rational or irrational Miller indices: correspondingly, the modulated structure is commensurate (superstructure) or incommensurate. In direct space, the modulated structure can be described in terms of displacive and/or occupation modulations with respect to the basic structure [1, 2].

On the other hand modular structures are built by one or more types of building modules (layers, slabs, rods etc.): series of structures are obtained by juxtaposing a different number of building modules, according to a general pattern $(B_1)_{n1}(B_2)_{n2}(B_3)_{n3}$ ... $(B_p)_{np}$ [3, 4].

Polytypes share some of the features of both modulated structures and modular structures: they are in fact built by stacking one or more types of layer along one direction (the stacking direction), resulting in a commensurate modulated structure (superstructure). Although the modulation is not as complex as in the case of incommensurate structures, the structure of the building layer itself is often quite complicated and a direct structure solution from the diffraction pattern is normally impracticable. An indirect, more sophisticated approach is thus required, able to exploit the symmetry features of the layer and of its stacking pattern, allowing the derivation of the stacking sequence knowing the structure of the building layer. A concrete example is here described that concerns a long-period polytype of mica, a group of minerals in which the most complex polytypes have been reported.

2. The Structure of the Micas and the Origin of the Phenomenon of Polytypism in the Micas

The crystal chemical unit of micas is a layer about 10 C thick (M layer), consisting of two tetrahedral (T) sheets sandwiching an octahedral sheet (O), between which interlayer cations occur [5] (Fig. 1). Each sheet has a nearly trigo-nal symmetry; however, because of the intralayer stagger [|a|/3 in (001) projection] between the two Tsheets, the highest layer-symmetry of the entire M layer is C12/m(l) [6] (layer-group notation after [7]).

For the geometrical description of the polytypism, the structure of micas is best visualized in terms of OD packets. OD stands for "Order-Disorder" and indicates that the stacking of layers may produce both periodic ("ordered") and non-periodic ("disordered") structures. It has no relation with the chemical order-disorder phenomena [8]. An OD packet corresponds to half an M layer plus half the plane of the interlayer cations, and constitutes the smallest continuous part, periodic in two dimensions, representing fully the chemical composition of a polytype [9, 10]. OD packets are polar and are indicated by the characters P_{2j} (packet pointing +c) and q_{2j+1} (packet pointing -c) (Fig. 1). Pairs of OD packets are related by symmetry operations that, in general, are valid in a subspace of the crystal space only (*local symmetry operations*, opposed to *global symmetry operations*, valid in the entire crystal space), and as such do not appear in the space-group type of the polytype. The set of all the local and global symmetry operations constitutes a *space groupoid* [11, 12].

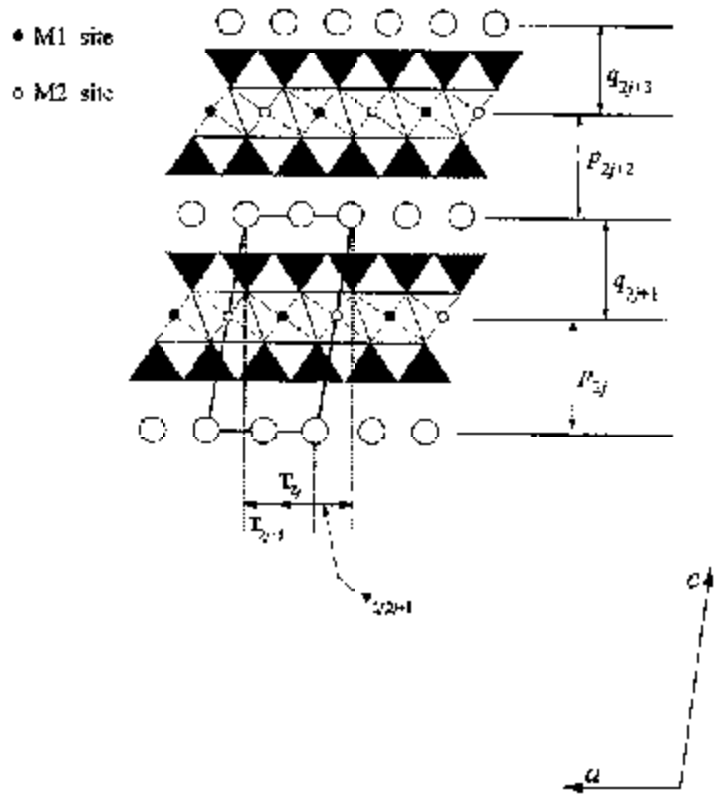

Fig. 1. Schematic representation of a slab b/4 thick, showing two layers of the 1M polytype. The M layer and the OD packets are shown.

Three translationally independent cation sites (M sites) are present in the O sheet: one (M1) has two OH groups in *trans*, whereas the other two sites (M2 and M3) have two OH groups in *cis*. On the basis of the occupation of these three octahedral sites, micas are classified into three *families*: *homo-octahedral* (all the three M sites have the same cation content), *meso-octahedral* (one M site is differently occupied from the other two), and *hetero-octahedral* (all the three M sites are differently occupied). Each family is then subdivided, on the basis of the rotations between q_{2j+1} and p_{2j+2}, into three groups: *subfamily A polytypes* [only $2n \times 60°$], *subfamily B polytypes* [only $(2n+1) \times 60°$ rotations], and *mixed-rotation polytypes* [both $2n \times 60°$ and $(2n+1) \times 60°$ rotations] [10, 13-15].

The stacking sequence of mica polytypes is described in terms of symbols and vectors giving the absolute space orientation of each OD packet, and the packet-to-packet displacement. The symbols consist of a sequence of characters referring to one period, placed between vertical bars; two lines of characters are used: the first line indicates the orientation of each packet with reference to a space-fixed axial setting, and the second line the packet-to-packet displacements. A dot " · " (homo- and meso-octahedral family) or a prime (') or double prime (") to indicate the chirality of the layer (hetero-octahedral family) separates the two packets of the same M layer:

$$T_0 \cdot T_1 \;\; T_2 \cdot T_3 \ldots$$
$$v_{0,1} \;\; * \;\; v_{2,3} \; * \ldots$$

where T_j 0-5, $v2_{j,2j+1}=\mathbf{T}_{2j}+\mathbf{T}_{2j+1}$ (**v**, **T** are the vectors corresponding to v and T characters, and the vector sum has to be taken *modulo* primitive hexagonal cell). <*> indicates null vector (no displacement: the packets q_{2j+1} and p_{2j+2} are bounded by the interlayer cations). The parity of the orientational characters is necessarily opposite to that of the displacement characters. In the meso-octahedral and hetero-octahedral families, the $v_{2j,2j+1}$ characters in the second line follow unequivocally from the T_{2j},T_{2j+1} ... characters in the first line; in the homo-octahedral family there are only two distinguishable orientations of the packets (even and uneven) [10, 14]. Simplified one-line symbols can thus be adopted:

Family	Complete symbol	Simplified symbol
Hetero-octahedral (one of the two enantiomorphs is indicated)	T_0 ‘ T_1 T_2 ‘ T_3 ... $v_{0,1}$ * $v_{2,3}$ * ...	$\|T_0$ ‘ T_1 T_2 ‘ T_3...$\|$
Meso-octahedral	T_0 A T_1 T_2 A T_3 ... $v_{0,1}$ * $v_{2,3}$ * ...	$\|T_0$ A T_1 T_2 A T_3...$\|$
Homo-octahedral (the case of packets with uneven parity is shown)	u A u u A u ... $v_{0,1}$ * $v_{2,3}$ * ...	$\|v_{0,1} * v_{2,3} * ... \|$

Layers in which the two packets P_{2j} and q_{2j+1} have the same or a different orientation (however with the same parity, to preserve to octahedral coordination of the cations) are termed Ml and M2 layers, respectively. The Ml layer is much more common, but several examples of micas built by the M2 layer are also known, and this type of layer is supposed to play an important role in the formation of long-period polytypes [16] (Fig. 2).

3. The Diffraction Pattern of Mica Polytypes

In the diffraction pattern of mica polytypes, systematic non-space-group absences extensively appear which derive from the existence of local symmetry operations relating pairs of packets. These absences are explained by the OD theory, and play an important role in the process of polytype identification.

If two or more identical copies of the same polytype are translated by a *superposition vector* (i.e. a vector corresponding to a submultiple of a transla-

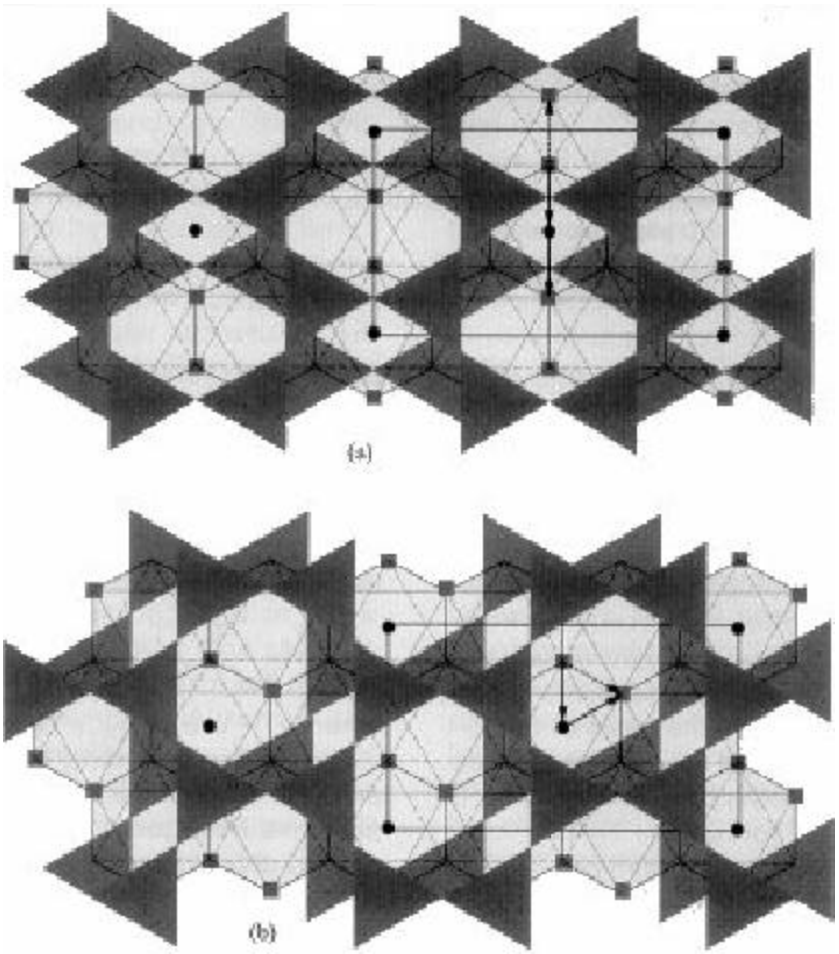

Fig. 2. The (001) projection of an M1 (a) and M2 (b) layer. Close circles indicate the origin of the O sheet, according to Šurovi… et al. (1984) (site with different occupation in the meso-octahedral family; site with lowest electron density in the hetero-octahedral family). Grey squares indicate the OH/I positions [overlapped in the (001) projection]. Thick arrows represent orientational (solid) and displacement (dotted) vectors. The orthohexagonal mesh in the (001) plane is also shown.

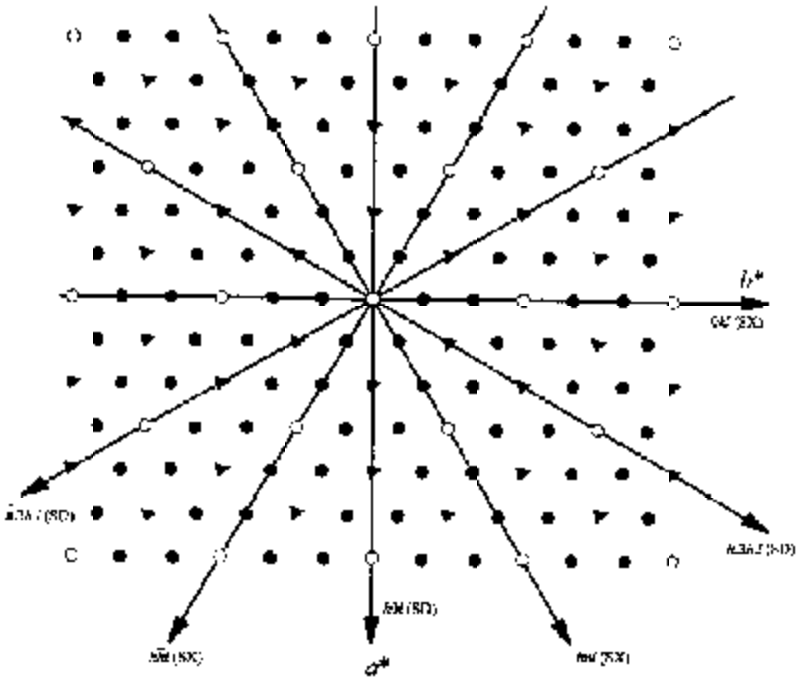

Fig. 3. (001) projection of mica reciprocal lattice. Open circles: S rows; triangles: D rows; close circles: X rows. The six central planes (three SD and three SX) that can commonly be recorded by the precession method are indicated (modified after [22]).

tion period) and superposed, a fictitious structure is obtained, which is termed superposition structure. Among the infinitely many possible superposition structures of a family, that in which all the possible positions of all layers are simultaneously realized is termed family structure and is common to all polytypes of the same family [17].

The weighted reciprocal lattice of a polytype can be decomposed into a sublattice (the family weighted sublattice, which is the Fourier transform of the family structure) and one or more cosets. The reflections building the family sublattice are termed family reflections and are ideally identical in position and intensity for all polytypes, both ordered (periodic) and disordered (non-periodic), belonging to the same family. The family reflections reveal the symmetry of the family structure, i.e. the symmetry principles governing the stacking mode in each polytype. The non-family reflections are instead characteristic of each polytype and reveal the individual stacking sequence: they are sharp for ordered polytypes, but streaked for disordered polytypes. The stacking sequence of a mica polytype can be obtained from the intensity distribution along reciprocal lattice rows parallel to c* provided that the structure of the ideal building layer is known. These rows are usefully classified into three kinds, labelled S (h=3n, k=3n), D (h:≠3n, k=3n) and X (k≠3n); reciprocal central planes (planes which have in common c*), are then classified, on the basis of the rows they contain, into SD and SX [18] (Fig. 3). The S rows are family rows common to all polytypes of the same family, whereas the D rows are family rows common to all polytypes of the same family and of the same subfamily (either A or B); they are instead non-family rows for mixed-rotation polytypes, and are thus characteristic of each mixed-rotation polytype. Finally, the X rows are non-family reflections for all polytypes and thus are characteristic of each polytype. If N is the number of layers in the unit cell, the reflections conditions along the three types of rows are:

1. **S rows**: one reflection out of N always appears, on the perpendicular to c* passing through the origin.

2. **D rows**: one reflection (family reflection) out of N appears for subfamily A polytypes, two (family reflections) for subfamily B, and N (non-family reflections) for mixed-rotation polytypes.

3. **X rows**: N reflections appear (non-family reflections) for all polytypes.

The D rows reveal the symmetry principle (practi-cally, the parity of n in the n×60° rotations),

whereas the intensity distribution along X rows permits to identify the stacking sequence by comparing the theo-retical and experimental values of the *Periodic Intensity Distribution* (PID) function along X rows [19-22]. The PID is the Fourier transform of the stacking sequence, obtained by removing the modulating effect of the single-layer transform from the structure factor:

$$S^N(hkl) = \frac{G^N(hkl)}{G_0(hkl)} \qquad (1)$$

where G^N is the Fourier transform of an N-layer polytype and G_0 is the Fourier transform of the single layer. In principle G_0 depends upon the layer orientation. However, in a subspace of the reciprocal space G_0 is almost identical for all the six possible layer orientations: Eq. (1) is always obeyed at least in the three planes 0kl, hhl and $\bar{h}$hl (for details see [22]). The possible stacking sequences for a given number of layers are obtained as described in [23], and from them the theoretical PID is computed [21]. The theoretical PID sequence that best matches the experimental one individuates the correct stacking sequence.

From the PID analysis, only the sequence of the displacement vectors $V_{2j,2j+1}$ is obtained. This is because the PID is actually the Fourier transform of the stacking sequence in case of all M1 layers. For polytypes containing M2 layers, the PID gives an approximate solution, which corresponds to substituting all the M2 layers with the corresponding Ml layers: the characters $T_{2j} \cdot T_{2j+1}$ or $v_{2i,2j+1}$ T_{2j} ' T_{2j+1} are replaced by the characters $e \cdot e$ $v_{2i,2j+1}$ $v_{2j,2j+1}$ or $u \cdot u$ $v_{2i,2j+1}$,depending on the parity of T_{2j} and T_{2+1j}. Since there is no difference between Ml and M2 layers in the homo-octahedral family, the approxima-tion of assuming all Ml layers is termed *homo-octahedral approximation* [22]. There is an n→l relation (relation of homomorphy) between hetero- or meso-octahedral polytypes and homo-octahedral polytypes: the n stacking sequences which are transformed into the same homo-octahedral sequence when considering only the parity of the orien-tation characters are thus said to be homomorphous to it. For the meso- and hetero-octahedral family, as well as for the distinction between the two members of an enantiomorphous pair, a complete structure refinement is necessary. However, only the structural models corresponding to polytypes homomorphous to the homo-octahedral sequence obtained by PID analysis need to be considered.

4. Experimental Investigation of Mica Polytypism

With the development of the imaging plate methodology, new impulse has been given to the moving film methods. The linearity between measured intensity and blackening of the film, the high-speed of the measurement, and the possibility of performing image analysis and data processing directly on a CRT are features particularly suitable for PID analysis. The precession method, combined with the imaging plate methodology, permits a rapid derivation of the PID from the intensities measured on undistorted images of the reciprocal lattice.

The crystal has to be mounted so as to have the (001) plane perpendicular to the goniometer rotation axis. This is not the common mounting for monoclinic crystals, which are usually oriented as to have the unique axis coincident with the dial axis. However, since the stacking of layers in micas is along c and the periodicity in reciprocal space appears along c*, it is necessary to have c* in all the images, i.e. to have c* aligned with the dial axis.

The radiation to be employed initially can be Mo or Cu. Mo is preferable for making easier the orientation of the crystal, but its wavelength is too short for the study of long-period polytypes, resulting in an insufficient resolution be-tween two successive reflections. Cu radiation is suitable for longer period polytypes (up to 10-12 layers) but it may be useless if the specimen contains too much Fe. The choice of the radiation to employ initially is thus the result of a compromise between the ease of orienting the crystal (Mo) and the eventuality of needing to change the target to get enough resolution. With some practice the orientation of a mica crystal on the precession camera becomes an easy task with Cu radiation, which can thus be selected as the best compromise in most cases. For longer period polytypes, Fe or Cr radiation becomes necessary to get sufficient resolution, once the crystal is oriented.

The identification of the stacking sequence of a mica polytype by PID analysis does not require, in general, intensity reduction for Lorentz-Polarization and absorption. This is because the PID function uses the relative intensities, and is computed in a 0.1 C^{-1}

repeat, within which the variation of the absorption is small. Besides, the weighted PID computed along several repeats is normalized in order to have both computed and measured values expressed on the same scale:

$$\sum_{j=1}^{N}\left[S_j^N\left(\hat{hkl}\right)\right]^2 = N^2 \qquad (2)$$

so that possible uncertainties are further reduced. Finally, the stacking sequence is determined by the best match between the computed and experimental PID. In case of precession motion, however, the Lorentz-Polarization effect is rather severe and must be taken into account.

To apply PID analysis the presence of twinning must be preliminary investigated, because the diffraction pattern of a twinned mica polytype may simulate the diffraction pattern of a different, untwinned polytype ("apparent polytypism" [24]). The analysis of twinning in micas exploits the geometry of the diffraction pattern and is described in details in [15]. The consequences of a wrong assumption about the presence/absence of twinning are given in [25]. For investigating the possibility of apparent polytypism one SD central plane and three SX central planes should be recorded. From these planes the geometry of the diffraction pattern can be analyzed on the basis of the criteria given in [15]. If the crystal is not twinned, the stacking sequence in the homo-octahedral approximation can be obtained from the PID along one or more X rows. This is the final stacking sequence if the polytype is built by all M1 layers, otherwise it represents the homomorphous equivalent of the correct stacking sequence. In both the meso- and the hetero-octahedral families, the final stacking sequence can be obtained only from a complete structure refinement, since the occupancies of the octahedral sites, and the sizes of the corresponding octahedra, have to be refined. Unluckily, micas almost invariably give broadened, oval shaped reflections, because of their platy morphology, which often is deformed and kinked. For this reason, quite often the quality of the sample is not sufficient to allow a data collection, and only the stacking sequence of the homomorphous polytype (PID stacking sequence) can be obtained.

5. Example

To illustrate concretely the process of identification of long-period mica polytypes, the example of the oxybiotite-$8A_2$ taken from [25] is here briefly summarized. The sample investigated consists of oxybiotite crystals from Ruiz Peak (New Mexico), whose main features are de-scribed in [26-28]. The specimen, of about 0.4 x 0.2 x 0.05 mm., was selected by direct inspection of single crystals under polarizing microscope. Observation in clove oil (refractive index 1.531) did not suggest the presence of twinning, to be however confirmed through the analysis of the geometry of the diffraction pattern.

The experimental diffraction study was performed with Cu radiation and a Ni thin foil as a filter to remove Kβ peak. Operating voltage and current were 35 kV and 15 mA respectively. Diffraction was recorded on Imaging Plate (IP) and transformed to digital format by a Rigaku R-AXIS DS2 laser reader. Intensities were then measured by using the Rigaku R-AXIS software package. The Lorentz-Polarization correction was calculated by using the equations developed by Waser [29].

The single-layer Fourier transform (Go in Eq. 1) was calculated by employing the atomic coordinates of the 1M polytype from the same sample [28], by using the ORFLS program [30] as modified by Takeda [19].

Figure 4 is the diffraction pattern from the hOl SD plane. The presence of only one reflection in the c_1^* repeat along D rows [h≠0(mod3)] clearly shows that the polytype under investigation belongs to subfamily A (only 2n x 60° rotations between q_{2j+1} and p_{2j+2}). Figure 5 shows the diffraction pattern from the *h*hl SX plane. The geometry of the diffraction pattern clearly shows that the polytype is not orthogonal. Non-orthogonal polytypes may undergo twinning by reticular pseudo-merohedry. The diffraction pattern of non-orthogonal twinned micas can be mistaken for that of a polytype with a number of layers multiple of 3 [18, 31-32]. Since the diffraction pattern of the sample under investigation shows eight equally-spaced reflections in the repeat corresponding to the single-layer period along the X (non-family) rows [h≠0(mod 3)], it follows that the crystal is not twinned, but consists of an 8-layer polytype. Out of 9212 possible 8-layer polytypes, only 94 belong to subfamily A [26]. Comparison of theoretically computed and experimentally recorded PID values had thus to be performed only for the 94 subfamily A polytypes. The stacking sequences of these 94 polytypes have been generated by PTGR program [23], and the corresponding PIDs have been computed by PTST98 program [22], in which the

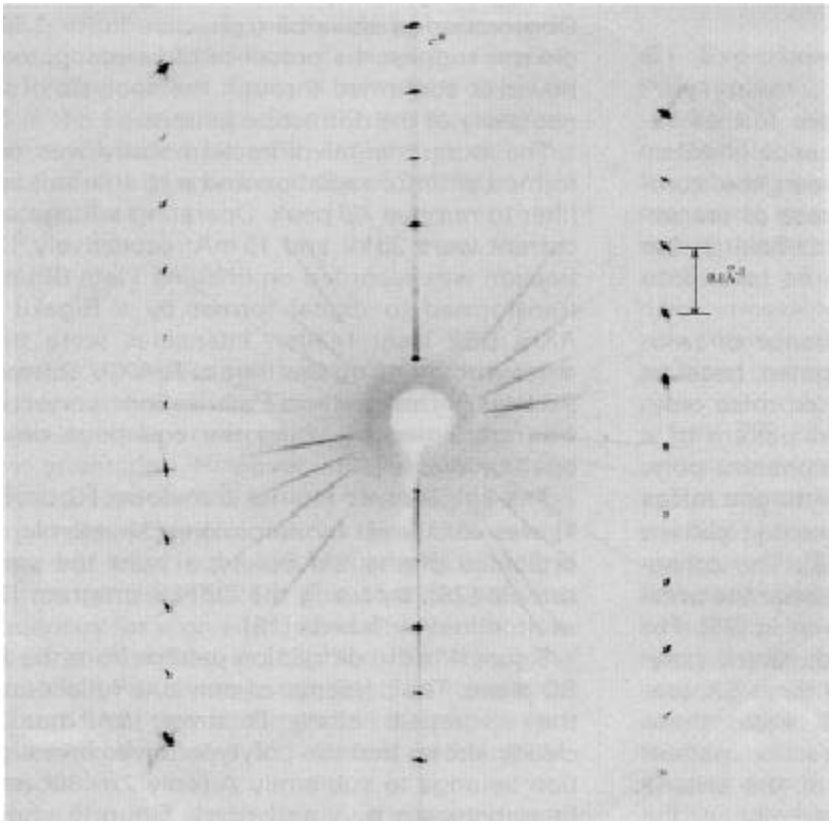

Fig. 4. Diffraction pattern from the h0l SD plane of the $8A_2$ polytype (only the first D rows have been recorded because CuKα was employed). The 0.1 C^{-1} interval corresponding to the single-layer period is indicated. The presence of a single reflection shows that the polytype belongs to subfamily A (modified after [25]).

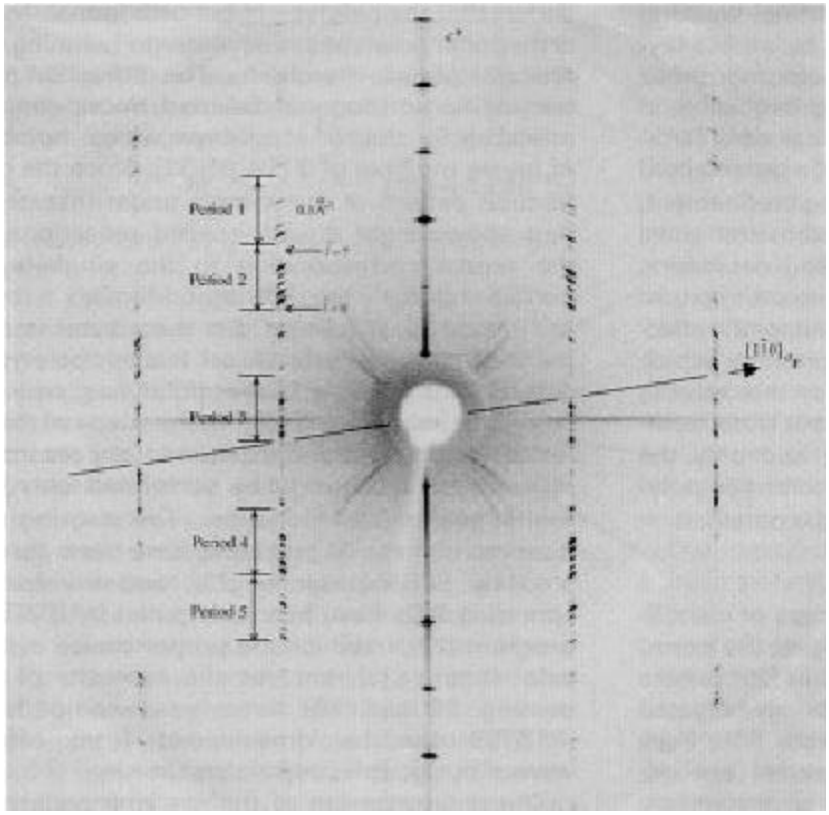

Fig. 5. Diffraction pattern from the $\bar{h}hl$ SX plane of the $8A_2$ polytype (only the first two X rows have been recorded because CuKα was employed). The $[1\bar{1}0]^*$ axis is traced according to the general theory of the axial settings for mica polytypes [31]. PID has been obtained from the intensities measured along the five periods indicated in the figure (modified after [25]).

proper choice of the axial setting [33] removes the necessity of re-peating 2N (ie. 16) times each comparison (PTST98 can be downloaded from http://www.nirim.go.jp/~nespolo/ptst.htm).

The determination of the stacking sequence has been performed by comparison of measured and computed PID values. For subfamily A polytypes with a number of layers not multiple of 3 the following symmetry relation holds [22]:

$$S^N\left(0,2k,\hat{l}\right) = S^N\left(\overset{\pm}{k},\bar{k},\hat{l}\right) = S^N\left(k,k,N-\hat{l}\right) \quad (3)$$

$$\hat{l} = l(\mathrm{mod}\, N)$$

It is thus enough to compute PID from the measured intensities in one of the reciprocal lattice planes containing non-family reflections. Physical defects of the crystal result in broadening and doubling of the reflections. The SX plane containing reflections of the best quality has thus been selected, namely $\bar{h}$hl. Then, in order to minimize the effect of the experimental errors, PID has been calculated from five periods along the $\bar{1}$1/X row (Table 1) and a mean value has been obtained (Table 2). Two of the periods in the diffraction pattern in Figure 5 have not been used. They correspond to regions including very faint reflections, where the Fourier transform of the single layer undergoes a sign change and where PID values are thus less reliable [22].

The PID computed from the stacking sequence of the 94 different polytypes has been compared with the experimentally measured PID and the degree of matching has been evaluated by means of an R factor defined exactly in the same way as for the structure factors, namely:

$$R_{PID} = \frac{\sum_{j=1}^{N}\left|S_j^N(hkl)_O - S_j^N(hkl)_C\right|}{\sum_{j=1}^{N} S_j^N(hkl)_O} \quad (4)$$

The best match corresponded to R_{PID}=0.04 (computed PID values for this sequence are in Table 2); the second best match to R_{PID}=0.33. This clearly shows that the stacking sequence has been uniquely identified. By employing the cell dimensions of the refined 1 M polytype from the same sample [281, the

Table 1. Derivation of PID from measured intensities of $8A_2$ polytype. Observed structure factors (Fo) have been obtained from the intensities measured in five periods along the $\bar{1}$1/X row. SLFT stands for Single Layer Fourier Transform.

Period	l (mod 8)	Fo	SLFT	Fo/SLFT	PID
1	7	.25	12.9925	.0192	.02
	6	.25	16.7667	.0149	.02
	5	83.33	20.6510	4.0352	4.44
	4	38.63	24.5330	1.5746	1.73
	3	47.01	28.2829	1.6621	1.83
	2	83.00	31.7709	2.6125	2.87
	1	168.75	34.8628	4.8404	5.32
	0	40.70	37.4274	1.0874	1.20
2	7	.22	39.3437	.0056	.00
	6	30.06	40.5091	.7421	.57
	5	183.05	40.8463	4.4814	3.47
	4	76.75	40.3088	1.9041	1.47
	3	91.39	38.8777	2.3507	1.82
	2	169.81	36.5677	4.6437	3.59
	1	246.62	33.4600	7.3706	5.70
	0	32.92	29.6496	1.1103	.96
3	7	24.77	12.4614	1.9877	1.46
	6	33.28	15.4120	2.1594	1.58
	5	111.86	17.6442	6.3398	4.65
	4	23.28	19.1113	1.2181	.89
	3	41.45	19.7841	2.0951	1.54
	2	60.84	19.6492	3.0963	2.27
	1	134.28	18.7094	7.1771	5.26
	0	30.39	16.9832	1.7894	1.31
4	7	18.80	22.0798	.8515	.52
	6	20.98	26.7785	.7835	.57
	5	172.90	30.9908	5.5791	4.07
	4	89.73	34.5793	2.5949	1.89
	3	99.68	37.4301	2.6631	1.94
	2	188.67	39.4573	4.7816	3.49
	1	288.53	40.5866	7.1090	5.19
	0	28.74	40.8295	.7039	.51
5	7	.22	40.2094	.0055	.01
	6	52.30	38.7837	1.3485	1.26
	5	172.66	36.6389	4.7125	4.42
	4	57.59	33.8844	1.6996	1.59
	3	51.37	30.6456	1.6763	1.57
	2	86.01	27.0555	3.1790	2.98
	1	129.75	23.2475	5.5812	5.23
	0	26.51	19.3487	1.3701	1.28

Table 2. Comparison of measured and computed PID of $8A_2$ polytype.

l (mod 8)	Period 1	Period 2	Period 3	Period 4	Period 5	Mean	Calculated
7	.02	.00	1.46	.62	.01	.30	.23
6	.02	.57	1.58	.57	1.26	.89	.90
5	4.44	3.47	4.65	4.07	4.42	3.98	4.07
4	1.73	1.47	.89	1.89	1.59	1.52	1.73
3	1.83	1.82	1.54	1.94	1.57	1.74	1.78
2	2.87	3.59	2.27	3.49	2.98	2.98	3.35
1	5.32	5.70	5.26	5.19	5.23	5.13	5.31
0	1.20	.86	1.31	.51	1.28	1.04	1.00

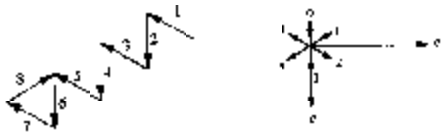

Fig. 6. The $v_{2j,2j+1}$ displacement vectors of the $8A_2$ polytype in the homo-octahedral approximation, as revealed by PID analysis of the diffraction pattern in Fig. 5. Axes of the space-fixed reference and vectors defining the orientation/ displacement of packets are shown on the right (modified after [25]).

approximate cell parameters of this polytype have been calculated through the axial transformations given in [33] and results are: a = 5.3 C, b = 9.2 C, c = 79.6 C, $\alpha = 90°$, $\beta = 91.3°$, $\gamma = 90°$.

The $v_{2j,2j+1}$ displacement characters describing the identified stacking sequence in the homo-octahedral approximation are 53535351 (Figure 6). This polytype was described in [21] with Ramsdell's [34] symbol $8A_2$ (polytype symmetry symbols according to [35]). The space group type is $C\bar{1}$, derived by applying the trans-formation rules for symbols given in [13].

6. Concluding Remarks

Modulated structures are receiving increasing attention in both the mineral realm and among synthetic compounds of technological interest. The imaging plate methodology is giving great impulse to the diffractional investigation by means of two-dimensional techniques, which are most suitable to record satellite reflections and the streaking typical of compounds with stacking disorder and modulation. In the case of commensurate modulate structures, specific approaches, like the OD theory of symmetry and the PID analysis of the intensity distribution of mica polytypes, permit to solve in a relatively simple way the structure of compounds which would be almost untreatable with classic methods of structure solution. A more systematic adoption of similar approaches in higher-dimensional spaces will likely bring an important contribution also in the investigation of incommensurate structures.

7. References

[1] A. Janner and T. Janssen, *Acta Crystallogr*., **A36**, 399 (1980).

[2] T. Jannsen, A. Janner, A. Looijenga-Vos, and P. M. de Wolff, *International Tables for Crystallography*, Vol. C., (Ed. A.C.J. Wilson and E. Prince). Dordrecht/Boston/ London: Kluwer Academic Publishers, 899 (1999).

[3] G. Ferraris, in Merlino, S. (Ed.) Modular aspects of minerals/EMU Notes in Mineralogy, vol. 1. Budapest: E`tv`s University press, 275 (1997).

[4] E. Makovicky, in Merlino, S. (Ed.) Modular aspects of minerals/EMU Notes in Mineralogy, vol. 1. Budapest: E`tv`s University press, 315 (1997).

[5] L. Pauling, *Proc. Nat. Ac. Sci.*, **16**, 123 (1930).

[6] A. Pabst, *Am. Mineral.*, **40**,967 (1955).

[7] K. Dornberger-Schiff, Acta Crystallogr., **12**, 173 (1959).

[8] K. Dornberger-Schiff, *Kristall und Technik*, **14**, 1027 (1979).

[9] S. Šurovi…, *Acta Crystallogr.*, **B30**, 6 (1974).

[10] K. Dornberger-Schiff, K.-O. Backhaus, and S, Šurovi…, *Clays Clay Miner*., **30**, 364 (1982).

[11] R. Sadanaga, R. and K. Ohsumi, *Acta Crystallogr.*, **A35**,115 (1979).

[12] K. Fichtner, *MATCH, commun. math. comput. chem.*, **9**, 21 (1980).

[13] K.-O. Backhaus and S. Šurovi…, *Clays Clay Miner.*, **32**, 453 (1980).

[14] S. Šurovi…, Z. Weiss and K.-O. Backhaus, *Clays Clay Miner.*, **32**: 454 (1984).

[15] M. Nespolo, *Mineral. J.*, **21**, 53 (1999).

[16] M. Nespolo, *Clays Clay Miner.*, **49**,1 (2001).

[17] S. Šurovi…, In G. Chapuis, and W. Paciorek (Ed.) Aperiodic '94. *Proceedings of the International Conference on Aperiodic Crystals.* Singapore/New Jersey/London/ Hong Kong: World Scientific, 595 (1994).

[18] M. Nespolo, G. Ferraris and H. Takeda, *Acta Crystallogr.*, **A56**,132 (2000).

[19] H. Takeda, *Acta Crystallogr.*, **22**, 845 (1967).

[20] H. Takeda and R. Sadanaga, *Mineral. J.*, **5**, 434 (1969).

[21] H. Takeda and M. Ross, *Am. Mineral*., **80**,715 (1995).

[22] M. Nespolo, H. Takeda, T Kogure and G. Ferraris, *Acta Crystallogr.*, **A55**, 659 (1999).

[23] H. Takeda, *Am. Mineral*., **56**,1042 (1971).

[24] Y. Takano and K. Takano, *J. Mineral. Soc. Jpn*., **3**, 674 (1958) (in Japanese).

[25] M. Nespolo and H. Takeda, *Mineral. J.*, **21**,103 (1999).

[26] M. Ross, H. Takeda and D. R. Wones, *Science*, **151**, 191 (1966).

[27] H. Takeda and M. Ross, *Am. Mineral*., **60**,1030 (1975).

[28] T. Ohta, H. Takeda and Y. Takduchi, *Am. Mineral.*, **67**, 298 (1982).

[29] J. Waser, *Rev. Sci. Instr.* **22**, 567 (1951).

[30] W. R. Busing, K. O. Martin and H. A. Levy, ORFLS, A FORTRAN Crystallographic Least-Squares Program. Oak Ridge National Laboratory, Tennessee, report ORNL-TM-305 (1962).

[31] R. Sadanaga and Y. TakJuchi, *Z. Kristallogr.*, **116**, 406 (1961).

[32] M. Nespolo and T. Kogure, *Z. Kristallogr.*, **213**, 4 (1998).

[33] M. Nespolo, H. Takeda and G. Ferraris, *Acta Crystallogr.*, **A54**, 348 (1998).

[34] L. S. Ramsdell, *Am. Mineral.*, **32**, 64 (1947).

[35] A. Guinier, G. B. Bokij, K. Boll-Dornberger, J. M. Cowley, S. Šurovi…, H. Jagodzinski, P. Khrisna, RM. De-Wolff, B.B. Zvyagin, D.E. Cox, P. Goodman, Th. Hahn, K. Kuchitsu and S.C. Abrahams, *Acta Crystallogr*. **A40**, 399 (1984).